United States Department of Commerce
Technology Administration
National Institute of Standards and Technology

NIST Technical Note 1383

Electromagnetic Shielding Characteristics of Optical-Fiber Connectors

Keith D. Masterson
David R. Novotny
Galen H. Koepke

TN 1383

Electromagnetic Shielding Characteristics of Optical-Fiber Connectors

Keith D. Masterson
David R. Novotny
Galen H. Koepke

Electromagnetic Fields Division
Electronics and Electrical Engineering Laboratory
National Institute of Standards and Technology
325 Broadway
Boulder, Colorado 80303-3328

April 1997

U.S. DEPARTMENT OF COMMERCE, William M. Daily, Secretary
TECHNOLOGY ADMINISTRATION, Mary L. Good, Under Secretary for Technology
NATIONAL INSTITUTE OF STANDARDS AND TECHNOLOGY, Robert E. Hebner, Acting Director

National Institute of Standards and Technology Technical Note
Natl. Inst. Stand. Technol., Tech. Note 1383, 44 pages (April 1997)
CODEN:NTNOEF

U.S. GOVERNMENT PRINTING OFFICE
WASHINGTON: 1997

For sale by the Superintendent of Documents, U.S. Government Printing Office, Washington, DC 20402-9325

CONTENTS

ELECTROMAGNETIC SHIELDING CHARACTERISTICS OF OPTICAL-FIBER CONNECTORS

Keith D. Masterson, David R. Novotny, and Galen H. Koepke

Electromagnetic Fields Division
National Institute of Standards and Technology
Boulder, CO

A number of commercially available optical-fiber connector styles (ST, SC, and FC) were tested to determine the extent to which their use in bulkhead adapter feedthroughs would compromise the shielding of electromagnetic interference for electronic enclosures. Metal, ceramic, and polymer components were included in the test matrix. Tests were carried out using a nested reverberation cell technique and cover a frequency range from 1 GHz to 16 GHz. The shielding effectiveness varied widely, from a low of about 20 dB to a high for an all metal FC connector system that was nearly equal to the 90 dB obtained for a blank reference plate. In some cases, the feedthrough coupled more energy into the enclosure than was coupled through the empty hole required to mount the adapter barrel. Comparison between the experimental results and the theory for coupling electromagnetic energy through a circular aperture enable us to more accurately determine the Q of the nested cell and to calculate transmission cross sections for the feedthroughs. The calculated transmission cross sections do not depend on the specific experimental parameters and can be used to estimate the degradation in shielding effectiveness for enclosures other than our reference cell. The inaccuracies in the reported transmission cross sections are calculated to be ±3 dB and are small compared to the differences between the measured cross sections.

Key Words: Electromagnetic interference; fiber optic adapter barrels; fiber optic connectors; fiber optics; shielding effectiveness

1. INTRODUCTION

Besides having very high bandwidths and low attenuation, optical fibers provide electrical isolation between system nodes, and they have found applications where the elimination of ground loops and common mode interference is the critical parameter. They are also characterized as being immune to electromagnetic interference (EMI). Although this is true for the fiber itself, the photodiode and laser diode optoelectronic transducers and their associated

electronic circuitry are very sensitive to EMI and must be placed in shielded enclosures with filtered supplies in order to fully realize this benefit in an environment of strong EMI. As bandwidths and data rates increase, we expect the problem of electromagnetic fields leaking into shielded enclosures to become more important. This is especially true for analog links used in demanding metrology applications such as often encountered at NIST. Although fiber feedthroughs consisting of very long, small diameter metal tubes which perform as waveguides below cutoff provide excellent shielding effectiveness for critical applications, they are more expensive and awkward to use than commercially available connectors and bulkhead adapters. It is expedient to use the commercially available products in many applications. The degree to which the shielding effectiveness of an enclosure is compromised by a particular connector is of considerable interest, especially for the newer, low cost polymer body styles.

We have been unable to find published data on this issue, although the EMI sensitivity of optoelectronic components have been studied [1]. We have experimentally measured the shielding effectiveness of a variety of commercially available connector systems. Our results are expected to be of considerable interest to engineers involved in designing optical-fiber links for critical applications, to provide baseline data for possible additional studies, and to aid the development of standard procedures to evaluate the shielding effectiveness of a variety of optoelectric components.

2. THEORY

Our goal is to determine the degradation in the shielding of an enclosure due to an optical-fiber bulkhead feedthrough mounted in one of the enclosure's walls. Since the shielding effectiveness of an enclosure is very dependent on its geometry and materials, we measure the degradation in a reference chamber when the feedthrough is installed and then calculate a transmission cross section for the feedthrough. This transmission cross section can then be used to estimate the shielding effectiveness of other enclosures that use the same connector system. We closely follow the work of Hill et al. [2], who studied the aperture excitation of large cavities. The experimental arrangement consists of nested, mode-stirred reverberation cells as shown in

figure 1. The cells perform much like common microwave ovens. Power radiated by the transmitting antenna A_T establishes an RF field between the cells. The stirring paddles assure that all modes are excited and the resultant fields are isotropic when averaged over time. Since mode stirring is more effective when the modes are closely spaced, reverberation cells are used for frequencies large compared to their fundamental mode. We list the practical lower frequency limits of our reverberation chamber and nested cell together with other pertinent data later in table 1.

Fields which leak into the inner cell give rise to a signal from the receiving antenna A_C. Because of the high RF reflectance and low losses for the cell walls, relatively high incident electrical fields can be established around the nested cell with modest input powers (>100 V/m with <10 W). Also, only a slight leakage into the nested cell results in a measurable field.

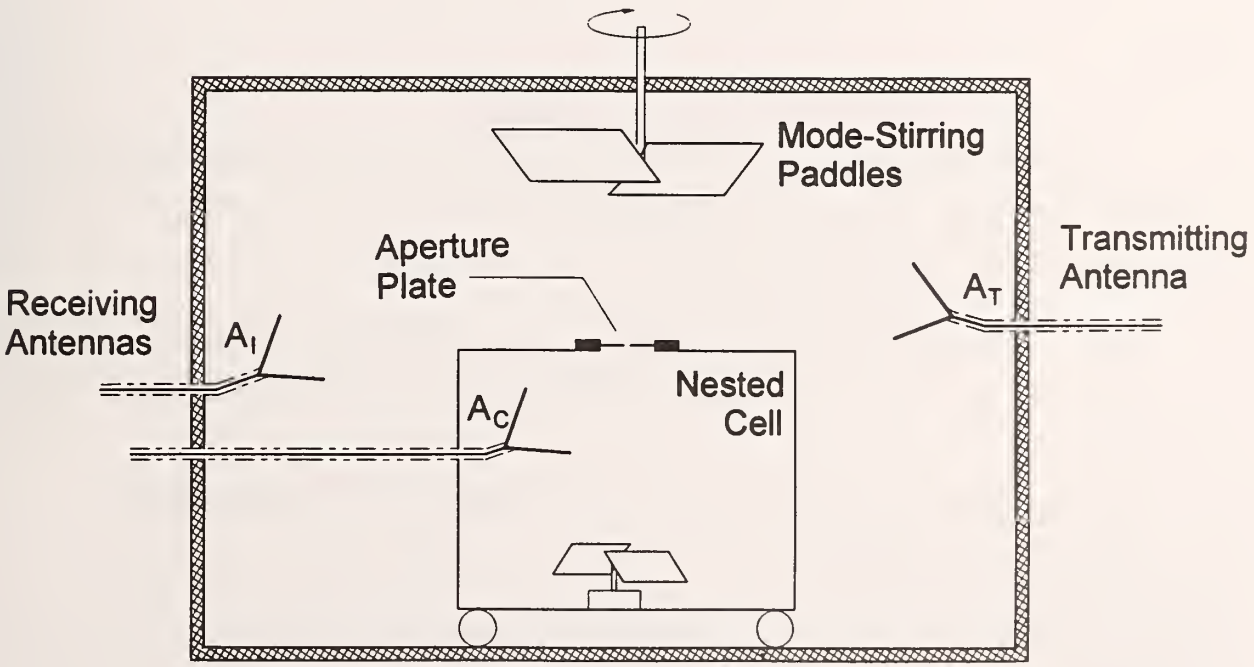

Figure 1. Configuration of reverberation chamber and nested cell for shielding effectiveness measurement

The shielding effectiveness of the enclosure is defined from the ratio of the power density S_I incident on the enclosure and monitored with the receiving antenna A_I to the power density S_C inside the enclosure and monitored with the receiving antenna A_C as

$$SE = 10 \log_{10} \left[\frac{S_I}{S_C} \right]. \tag{1}$$

If the enclosure contains no source, SE is always positive. The ratio S_I/S_C is given formally by

$$\frac{S_I}{S_C} = \frac{2kV}{<\sigma_T>} \frac{1}{Q} = \frac{2kV}{<\sigma_T>} \sum \frac{1}{Q_i}, \tag{2}$$

where

k = wave number of the incident EM radiation,

$<\sigma_T>$ = transmission cross section of the aperture averaged for uniform, isotropic incident radiation of wavelength $2\pi/k$,

V = the volume of the cavity,

Q = the quality factor for the electrical characteristics of the enclosure, and

Q_i = the contribution of a particular loss mechanism to the total Q of the enclosure.

From experimental measurements of S_I/S_C, V, and Q, we can determine the transmission cross section of the aperture. If the aperture is filled with an optical-fiber connector system, we can determine a transmission cross section for the connector system. This transmission cross section can be used to estimate the degradation in the shielding effectiveness of enclosures that might be used in practical systems.

For a high Q enclosure, Q is very sensitive to geometry, construction materials, and the specific experimental setup. An accurate determination of Q is difficult by either direct experimental qameasurements or theoretical calculations. However, by measuring the *SE* for a well defined small circular aperture and relating the results to the theoretically predicted values for the aperture, we can eliminate the cavity Q from eq (2) and determine values for the transmission cross sections of the various connector systems relative to that of the reference aperture.

The Q of the nested cell is determined by the rate of dissipation of the electromagnetic energy that is inside it. Each of the loss mechanisms contribute a component Q_i. These components can be calculated [2] and their relative magnitudes compared. The power dissipated by absorption in the enclosure walls is

$$Q_1 = \frac{3V}{2S}\left[\frac{kc\mu_O\sigma_w}{2\mu_r}\right]^{1/2}, \tag{3}$$

where V and S are the cavity's interior volume and surface area, σ_w and μ_r are the conductivity and relative permeability of the cavity's walls, and μ_O is the permeability of free space. The conductivity of the wall is the most difficult term to accurately determine. We use a value of 8.83×10^6 S/m, which was experimentally measured for an aluminum alloy similar to that from which our nested cell was fabricated [2].

The power dissipated by coupling into the receiving antenna is

$$Q_2 = \frac{2V}{m\pi}k^3, \tag{4}$$

where m is an impedance mismatch factor (m = 1 for a matched load, as was our case).

The power lost back through the aperture is

$$Q_3 = \frac{2V}{<\sigma_T>} k \ . \tag{5}$$

Although an exact solution for the transmission coefficient of circular apertures is available in terms of spheroidal functions [3], we use the following approximate solutions given by Hill et al. [2] for electrically small and electrically large circular apertures of radius *a:*

$$<\sigma_T>_S = \frac{16}{9\pi} k^4 a^6, \qquad \text{electrically small,} \tag{6}$$

and

$$<\sigma_T>_L = \frac{\pi a^2}{2}, \qquad \text{electrically large.} \tag{7}$$

Theoretical solutions for normal incidence which are based on variational approximations [4] show increases in the transmission cross section of up to 2 dB at $ka = 1.5$ (see Appendix B). Based on this work and the experimental data from Hill et al. [2], which also indicates the presence of an increase in the transmission cross section near $ka = 1.5$ for reverberation chamber measurements, we chose $<\sigma_T> = <\sigma_T>_S$ up to $ka = 1.4$ and then linearly connected this with $<\sigma_T> = <\sigma_T>_L$ for $ka \geq 5$, as shown in Appendix B.

Additional power can be absorbed by cable shielding and other materials placed in the enclosure leading to a contribution Q_4. We leave Q_4 to be determined by fitting theoretical curves to the experimental data for the well defined small circular apertures. We have evaluated $Q_{1,2,\text{ and }3}$ and plotted the results in figure 2. At frequencies below 1 GHz, the Q is dominated by the absorption of the receive antenna in the cavity, while at higher frequencies the wall losses dominate the net result.

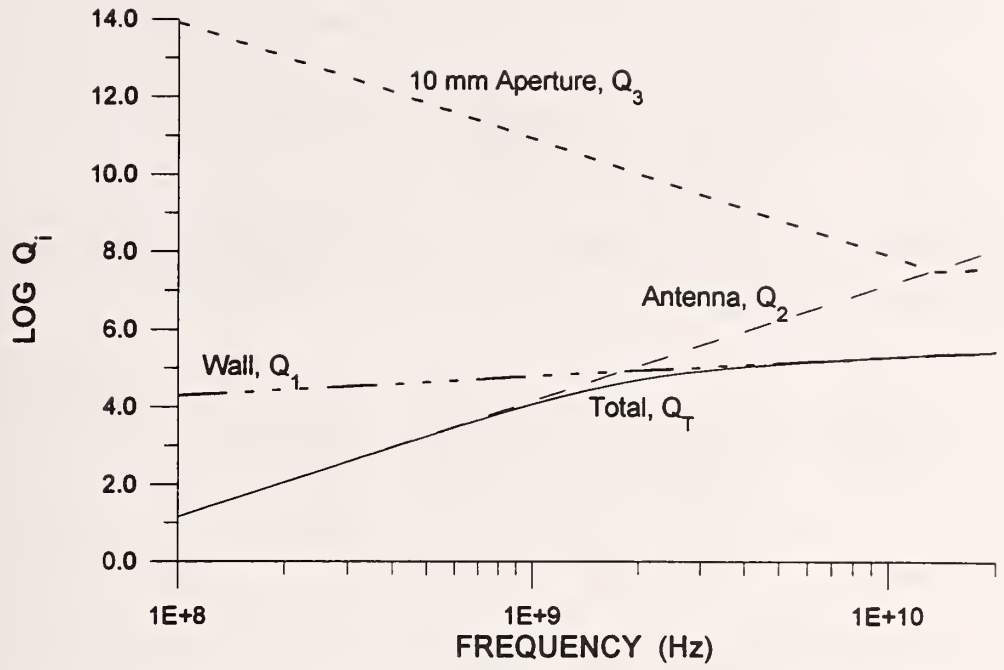

Figure 2. Q of the nested cell and contributions due to various loss mechanisms.

The transmission cross section for a bulkhead feedthrough can be calculated from eq (2) if the cavity Q is known. Using eq (2) and eq (5), we can express the shielding effectiveness as

$$\frac{S_1}{S_c} = \frac{2Vk}{\langle\sigma_T\rangle}\left[\frac{1}{Q_P}\right] + 1 \ , \tag{8}$$

where

$$\frac{1}{Q_P} = \frac{1}{Q} - \frac{1}{Q_3} \ , \tag{9}$$

and then eliminate Q_P by obtaining data for small circular apertures with known diameters while using the same experimental parameters. Thus, the measured transmission cross sections for feedthroughs can be expressed in terms of the theoretical values for the small open apertures as

$$\frac{<\sigma_T>_{FT}}{<\sigma_T>_{OA}} = \frac{(S_I/S_C)_{OA} - 1}{(S_I/S_C)_{FT} - 1} . \qquad (10)$$

The ratios of the power densities are obtained by applying calibration factors to the output of the spectrum analyzers as follows:

$$\frac{S_I}{S_C} = \frac{F_{1SA}\, F_{1C}\, F_{1AF}}{F_{2SA}\, F_{2C}\, F_{2AF}} \frac{SA_1}{SA_2} = \frac{R}{F} , \qquad (11)$$

where

F_{SA} = Calibration factor for the spectrum analyzer,
F_C = Calibration factor for cable loss,
F_{AF} = Antenna transfer function,
SA = Numerical output from spectrum analyzer, and
$R = SA_1 / SA_2$.

The calibration constant F is independent of the feedthrough system under measurement. The individual terms are displayed explicitly because the accuracy of the calibration factors must be considered later in the error analysis.

3. EXPERIMENTAL PROCEDURE

3.1 Apparatus

A diagram of the experimental setup is shown in figure 1. The larger, outer reverberation chamber and its use in more general EMI/EMC studies is described in more detail by Crawford and Koepke [5]. Its characteristics and the parameters under which we operated are summarized in table 1. The nested cell was constructed of welded aluminum with a large access door in the front that was sealed with a double row of finger stock, steel wool gasket strips, and conducting tape. Other characteristics of the nested cell are summarized in table 2.

Table 1. Characteristics of the reverberation chamber and the nested cell.

	Material	Dimensions (m)			Low frequency	Approx.
		Length	Width	Height	cutoff	Q
Large reverberation chamber	Painted Steel	4.57	3.05	2.74	~500 MHz	~10^5
Access door	"		1.23	2.13		
Stir paddles	Al alloy	~1.42	~0.71		irregular	
Nested cell	Welded Al alloy	1.48	1.16	1.43	~1 GHz	~10^5
Access door	Al alloy		0.63	0.78		
Stir paddles	"	0.61	0.46		rectangle	

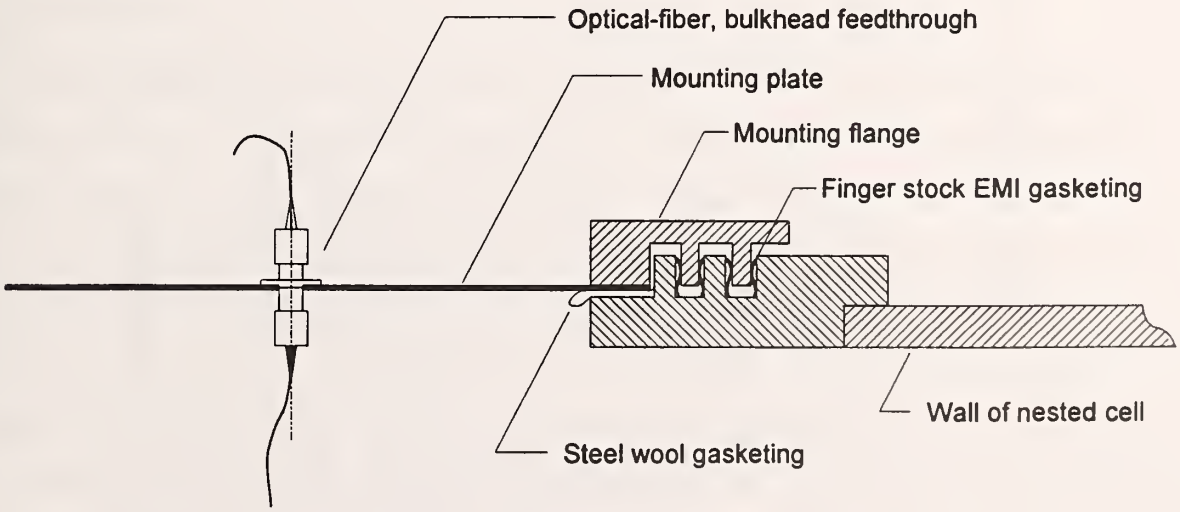

Figure 3. Detail of fixture for holding mounting plate in the nested cell.

Table 2. Typical operating parameters for the equipment.

Frequency range (GHz)		1-2	2-3	2.7-4	4-8	8-12	12-14	14-16
Ssignal generator (dB (1m W))		−25	−10	0	0	0	−4	−4
Amplifier gain (dB)		35	35	35	35	40	40	40
Mode stirring	Reverb chamber (rev/min)	12	12	12	12	12	12	12
	Nested cell (rev/min)	17	17	17	17	17	17	17
Spectrum analyzer S_1	Reference level (dB (1m W))	0	0	0	0	0	0	0
	Resolution bandwidth (kHz)	10	10	300	300	300	300	300
	Internal attenuation (dB)	10	10	10	10	10	10	10
	External attenuation (dB)	50	50	30	30	30	30	30
Spectrum analyzer S_c	Reference level (dB (1m W))	0	0	−20	−20	−20	−40	−40
	Resolution bandwidth (kHz)	10	10	10	10	10	10	10
	Internal attenuation (dB)	10	10	10	10	10	10	10
	External attenuation (dB)	0	0	0	0	0	0	0

The nested cell has a square port (255 mm each side) to which a test plate can be mounted. Figure 3 shows a cross section of the mounting frame with its double row of finger-stock seals to minimize unwanted leakage of electromagnetic energy. To further suppress leakage into the cell, we also placed a 30 mm wide strip of steel wool between the plate and the mounting frame as shown. We mounted the adapter barrels following the manufacture's recommended procedures in a 300 mm square test plate of 1.6 mm thick aluminum. No effort was made to increase the shielding by adding extra gaskets. However, before assembly all contact surfaces on the plate and cell wall were buffed with steel wool to remove oxide layers and improve the electrical contact.

The two broadband, open horn receiving antennas had frequency responses from 800 MHz to 16 GHz and were a matched pair. To obtain high EMI immunity for the lines between the nested cell and the outside bulkhead of the main reverberation chamber, we used semi-rigid coaxial cable. The DC line to the mode stir paddle in the nested cell was shielded and filtered. In order to minimize EMI into the nested cell and signal lines, all electrical connections were wrapped with steel wool and then covered with electrically conducting tape.

3.2 Test and Connector Matrix

We performed measurements on ST, SC, and FC/PC optical-fiber connector systems. These three styles are currently the most popular and readily available, and they represent the most cost-effective approach for optical-fiber links in many applications. The ST and FC/PC styles are also available in a variety of material combinations ranging from all dielectric to all metal. This provided the opportunity to study a number of variables that might affect the shielding effectiveness of the connector system. The principal components of a bulkhead feedthrough consisting of an adapter barrel and optical-fiber connectors are identified in the cross section of a representative installation shown in figure 4. The ST and FC styles include metal connector and adapter bodies with either stainless steel or ceramic ferrules and alignment sleeves, as well as polymer connector and adapter bodies with ceramic ferrules and alignment sleeves. The SC system is primarily of polymer and ceramic construction. However, we used

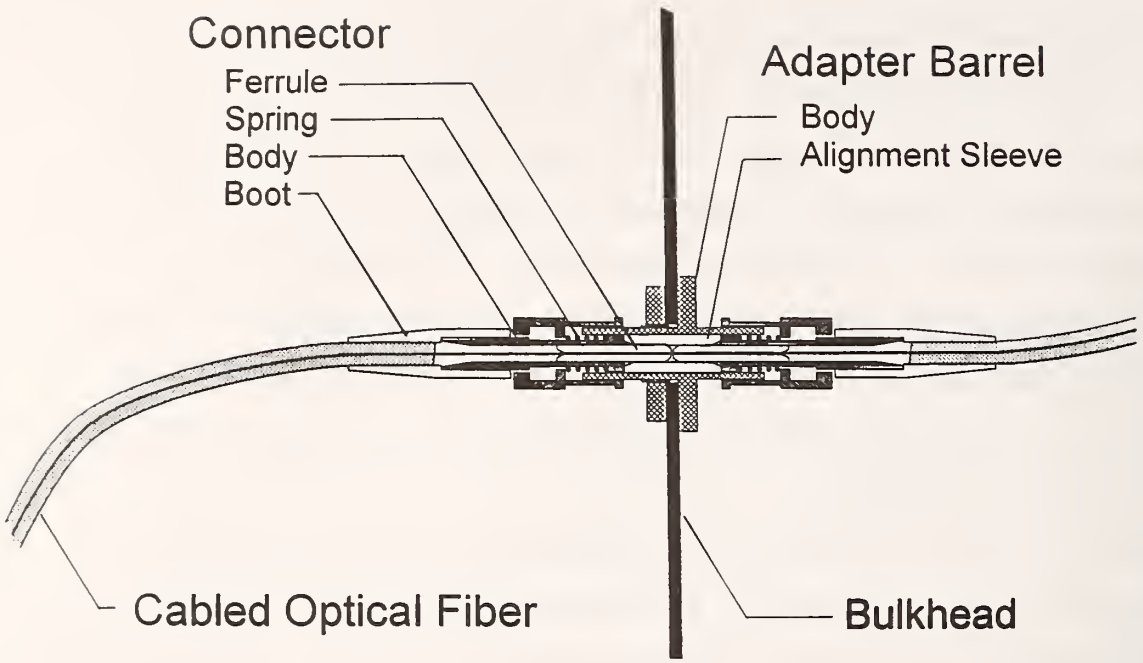

Figure 4. Cross section of typical connector-adapter barrel feedthrough.

SC adapter barrels with both metal and ceramic alignment sleeves. Limited resources did not permit us to test all the combinations. Instead, we tested representative all-metal and all-dielectric systems and then mixed some of the metal dielectric components to get an idea of the performance of systems that might occur in general usage. Table 3 lists the various connectors and adapter barrels that we tested together with their material components.

3.3 Data Acquisition

The instrumentation shown in figure 5 was used to accumulate data over 9 frequency bands. Many of the details for the experimental parameters are contained in table 2. The output signal from the tracking generator was amplified about 40 dB before being sent to the transmit antenna. Since appropriate power amplifiers cover about one octive in frequency range, it was necessary to continually switch between 6 power amplifiers to cover the entire 1 GHz to 16 GHz range. The power input to the chamber ranged from 3 W to 10 W.

Table 3. Connectors, components and materials used in test matrix.

SET	TYPE	CODE	CONNECTOR		ADAPTER BARREL	
			Body	Ferrule	Body	Alignment sleeve
1	ST	STMM	metal	stainless	metal	stainless
2	ST	STMP	metal	stainless	polymer	ceramic
3	ST	STPP	polymer	ceramic	polymer	ceramic
4	ST	STOA	9.5 mm dia. open aperture			
5	FC	FCMM	metal	stainless	metal	stainless
6	FC	FCMC	metal	ceramic	metal	stainless
7	FC	FCMP	polymer	ceramic	metal	stainless
8	FC	FCOA	9.0 mm dia. open aperture			
9	SC	SCPP	polymer	ceramic	polymer	ceramic
10	SC	SCPM	polymer	ceramic	polymer	metal
11	SC	SCOA	9.9 mm by 13.6 mm open aperture			
12	SC-DUP	SCDP	polymer	ceramic	polymer	ceramic
13	SC-DUP	SCDO	9.9 mm by 26.4 mm open aperture			
14	SC-DUP	SCDT	As in 12 but with long dimension bisected with 2 mm wide conducting strip			
15	REF	REF	Blank reference plate with no aperture			
16	Open Port	LGOA	0.25 m by 0.25 m open, mounting port			

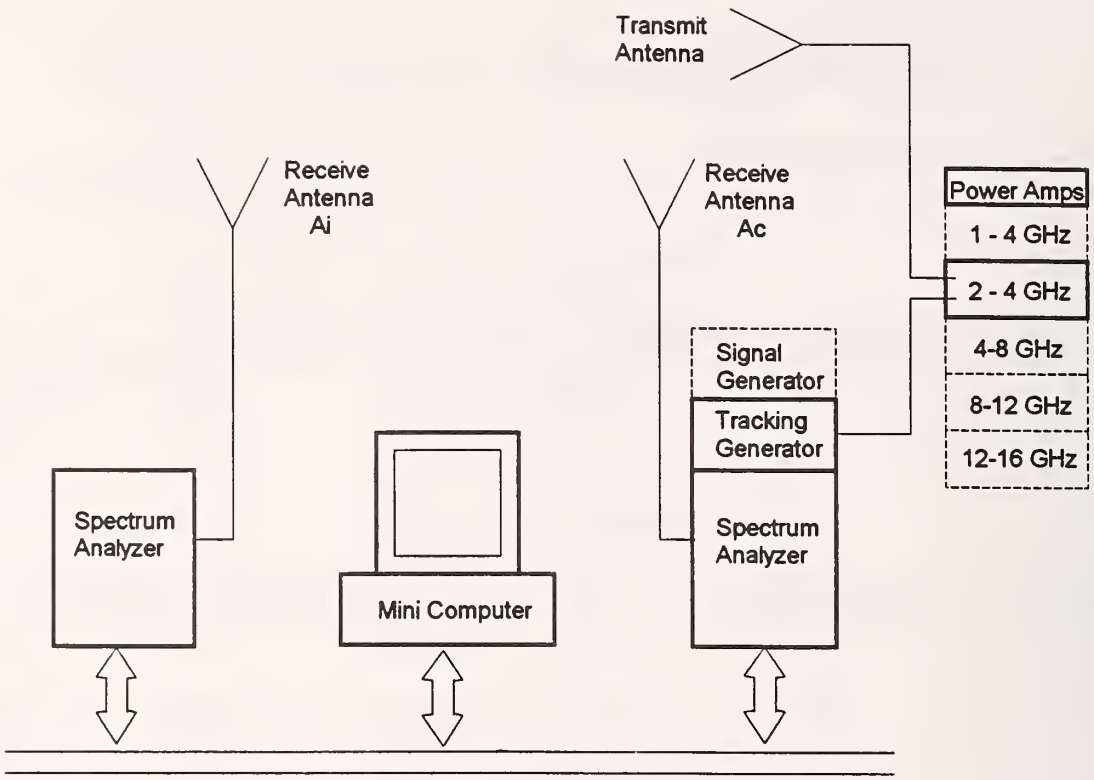

Figure 5. Instrumentation for data acquisition.

At frequencies above 3 GHz we used a mode-stirred technique where the input is repetitively swept across the frequency band while the metal stirring paddles are slowly rotated to mix the cavity modes and establish a field that when averaged over time is nearly isotropic. The low power signal from the receive antenna A_C inside the nested cell was accumulated by a spectrum analyzer with a tracking generator that supplied the input to the power amplifier. Since we could not synchronize a second spectrum analyzer with the tracking generator, the high power signal from the antenna A_I between the cell walls was recorded by a free-running spectrum analyzer. We accumulated data in a peak-hold mode on each spectrum analyzer and averaged long enough to ensure that mode and channel filling were almost complete. Although theoretical data for the transmission cross section more closely model an averaged signal, the approximate 8 dB increase in the signal obtained using the peak-hold method cancels when the ratio of the two signals is taken. After approximately 1 h of run time, no changes in the displayed signal were observable from sweep to sweep.

At frequencies below those accessible by the tracking generator, the input frequency was fixed, and the spectrum analyzers were left to accumulate signal over many paddle wheel revolutions. The frequency was stepped to the next desired value and the measurement was repeated. This generally results in somewhat more accurate data at the set measurement frequency, but allows the possibility of missing narrow resonances in the measurement. However, we do not expect to observe narrow resonances at the lower frequencies for the connector systems under study because their physical dimensions are much smaller than one wavelength. In this mode of operation, 2 h were required to obtain the data at the 21 frequencies which we used to span the 1 GHz to 3 GHz interval.

We first measured a blank reference plate with no aperture to determine the leakage into the nested cell and to establish a maximum SE that could be detected above the noise. Then a plate with an installed optical-fiber feedthrough was measured. Finally, without disturbing the mounting plate, we removed the connectors and adaptor barrel to leave just an open aperture in the plate and repeated the measurement. This provided data that could be compared to theory and used to adjust the calculated value for the Q of the nested cell. The total run time over the complete 1 GHz to 16 GHz frequency range totaled about 10 h for a single connector configuration.

The spectrum analyzers were recalibrated frequently according to the manufacturer's directions. Loss curves for the coaxial lines from the receive antennas to the spectrum analyzers were obtained by calibrating them on a network analyzer.

4. DATA ANALYSIS

Our goal is to use eq (10) to calculate the relative transmission cross sections from our shielding effectiveness measurements. The transmission cross sections for the small circular, open reference apertures computed from eq (6) and eq (7) are smooth featureless curves that can be compared to the experimental data. The experimental data from mode stirred reverberation chamber measurements is typically very noisy because of the statistical mixing of the many possible modes. Therefore, we averaged a large number of closely spaced data points to reduce

the noise. The initial spectral data contained over 7000 points between 2.7 GHz and 16 GHz. Calibration factors measured for the cable losses were applied, and the shielding effectiveness was obtained from eq (1). These data were then averaged by applying a second-order least-squares fit to sets of nine points and keeping the central point. We then stepped three points and repeated across the entire data set. This smoothing procedure was applied twice to reduce the data to about 700 points. Comparison of curves before and after smoothing shows little loss in sharp spectral features from this procedure.

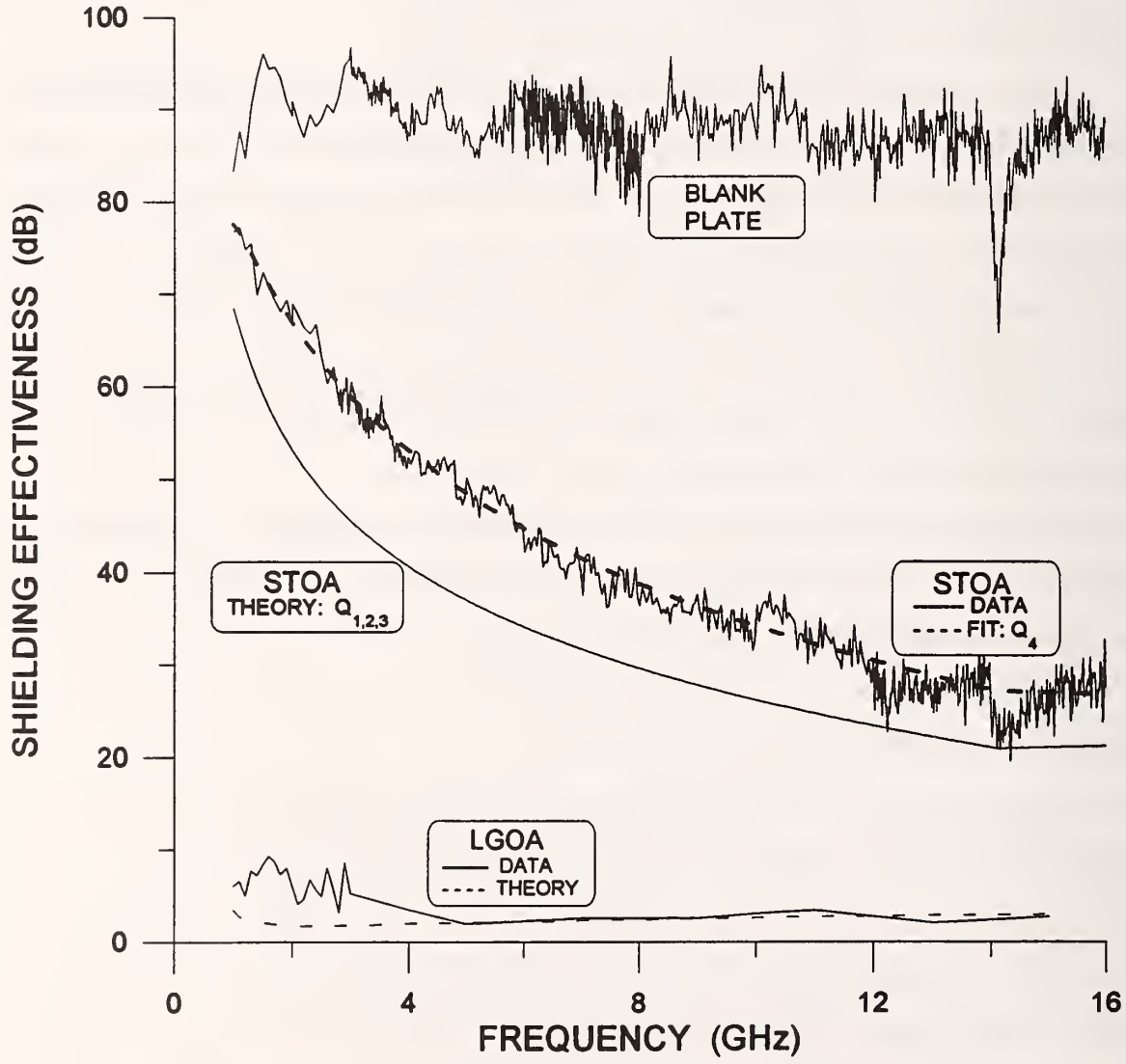

Figure 6. Reference values for the shielding effectiveness of the nested cell.

Figure 6 shows the resulting traces for the blank reference plate and a plate with the 9.5 mm diameter open aperture required to mount the ST bulkhead adapter. At the bottom of the figure, we have also included limited data we took for the shielding effectiveness of the large square mounting port (0.25 m by 0.25 m) which was left open and without a mounting plate. Over one portion of the curve for the blank reference plate, the unsmoothed data are shown to illustrate the effects of smoothing. This curve also shows a sharp dip at 14 GHz. This is attributed to a small gap or crack in the shielding which was resonant at that frequency and allowed some leakage into the cell.

The raw data also show occasional step-like jumps. The solid, smooth curves in figure 6 are the theoretically calculated values for the shielding effectiveness of the open apertures and do not predict any such jumps. The observed jumps always occur at the changes in the frequency bands where we physically changed the input and output cables to the power amplifiers. During this process, it was easy to bump the signal cables to the spectrum analyzer and slightly alter the signal coupled into it. Unfortunately, this was discovered late in the total measurement process and affects much of the data; the implications will be discussed in the section on error analysis. We have used the theoretical curves and the experimental evidence of the magnitude and direction of such jumps to correct the raw spectral traces for most cases where a short interval in the data was clearly out of step with the rest of the curve.

A smooth, continuous analytical expression based on the theory of small open apertures is desirable for SE_{OA} and $(S_1/S_C)_{OA}$ in order to remove the statistical fluctuations from the experimental data and allow interpolation for any desired frequency within the experimental limits. The solid curve labeled STOA in figure 6 is calculated from theory for the shielding effectiveness of the 9.5 mm aperture and lies about 7 dB below the experimental data. This implies the presence of additional losses that lower the Q of the nested cell, for example, due to higher than expected wall losses or absorption by materials that are in the cell. Absorption by steel wool that may have been left hanging from the lip of the mounting plate as shown in figure 3 appears to be especially significant. A mounting plate was installed following the same procedure used during the experimental testing, and we observed that in some places up to a centimeter of steel wool was left exposed. To account for the additional loss, we added the

term Q_4 to eq (2). We modeled the absorption as an electrically large aperture, roughly equal to the surface area of the exposed steel wool, and then used this approximation over all *ka* since its boundaries would not sustain the currents required to produce scattered fields included in the electrically small aperture approximation. The resulting theoretically calculated shielding effectiveness gave a much better fit to the observed data. In order to further increase the accuracy of the fit, we let

$$\frac{1}{Q_4} = \frac{A}{k^1} + \frac{B}{k^2} + \frac{C}{k^3} \tag{12}$$

and used a standard regression analysis [6] to determine the fitting parameters A , B, and C. The resulting fits match the experimental data well, as shown for the ST connector by the dashed line in figure 6. The fitting parameters for the ST, FC, and SC connectors are given in table 4. Variations in the fitting parameters for the open apertures arise from inaccuracies in the simple theory for describing the transmission of the various apertures, the amount of steel wool left exposed each time the mounting plate was replaced, and effects traceable to the faulty connector. In the case of the SC connectors, the apertures are rectangular. Still, our experimental data for the aperture required for the simplex connector is fit well by using a circular aperture of equivalent area. However, for the higher aspect ratio aperture required for the duplex connector, this only worked well for the electrically large approximation. For values of $ka < 1$, the shielding effectiveness for the duplex aperture is considerably reduced from that predicted by the equal area approximation, probably due to resonance effects. We placed a 1 mm wide piece of conducting copper-foil tape across the center of the long dimension of the aperture for the SC-duplex connector and repeated the measurements. The shielding effectiveness for $ka < 1$ was improved substantially, and the measured values were nearly equal to that expected from two single SC apertures.

We have collected all the curves for the shielding effectiveness of the nested cell with the various apertures and connector feedthrough styles into Appendix A.

The transmission cross sections for the reference open apertures were calculated from eq (6) and eq (7), and then the transmission cross sections for the various connector styles were

Table 4. Fitting parameters for open apertures.

Aperture	Parameter		
	A	B	C
ST	$-(2.83 \pm 3.68)\ 10^{-4}$	1.357 ± 0.064	-22.6 ± 1.9
FC	$-(2.8 \pm 1.3)\ 10^{-3}$	2.75 ± 0.14	-45.8 ± 2.8
SC	$(1.81 \pm 0.08)\ 10^{-3}$	1.013 ± 0.047	-9.63 ± 1.35

calculated from eq (10). The experimentally determined transmission cross sections for all the connector feedthroughs are presented in graphical form in figures 7, 8, and 9. Included as smooth curves in the figures are the theoretical values for the open apertures. The dashed curve is for the 9.5 mm open aperture and is included as a common reference in all the plots

The transmission cross sections for all the SC-duplex configurations are calculated using the transmission cross section and curve fit for the single SC connector as the reference. Although the transmission cross section for a high aspect ratio aperture appears to be predicted by using a circular aperture of equal area for $ka > 1.5$, we do not feel that this is accurate enough to be used as a reference for smaller value of *ka*. Since the shielding effectiveness of the duplex aperture with the conducting tape is close to that expected for two single SC apertures, we conclude that the experimental conditions for the mounting plate were very close to those for the single SC aperture. Therefore, we used the data of the single aperture as the reference for the transmission cross section of the duplex feedthrough.

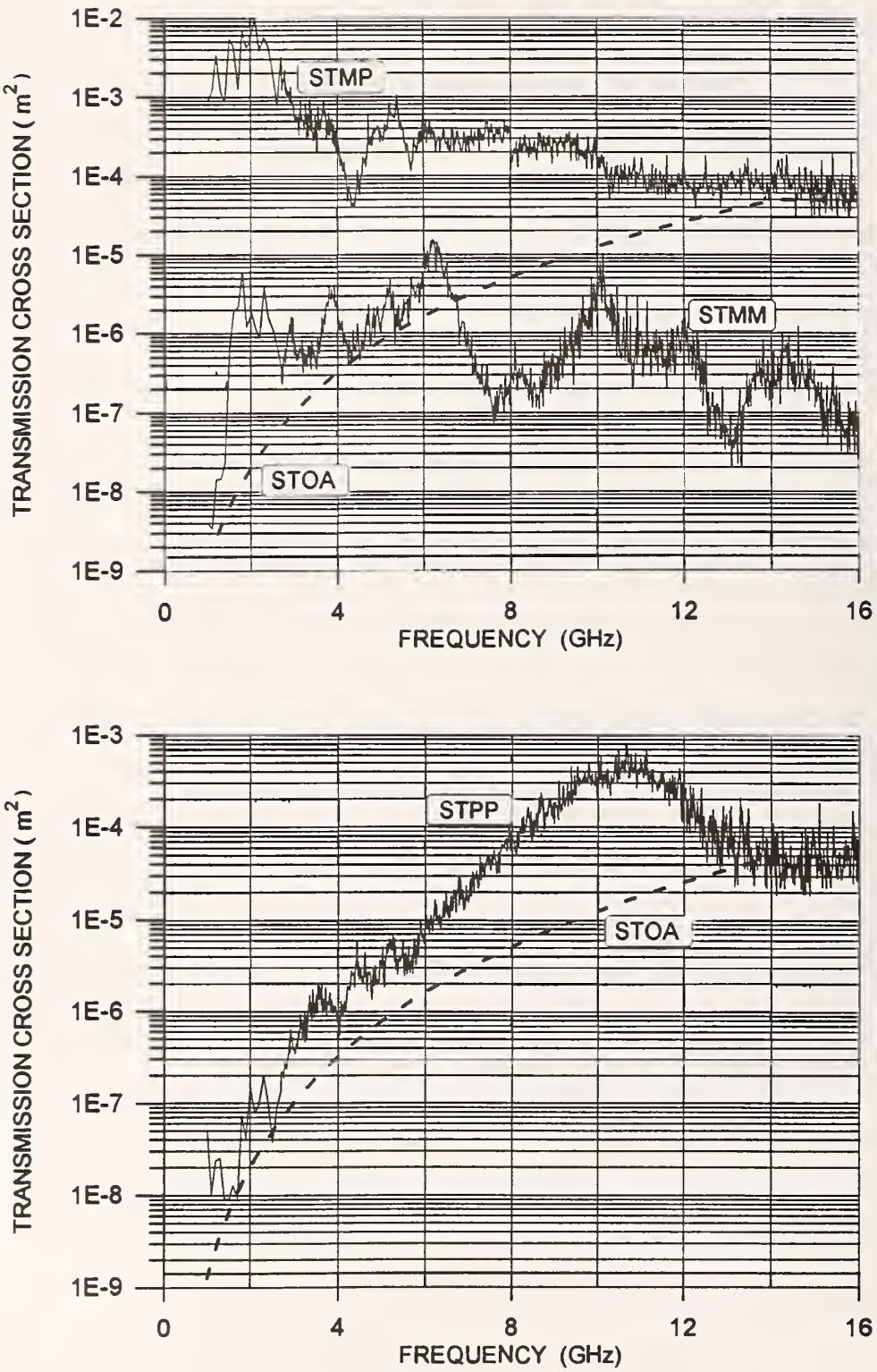

Figure 7. Transmission cross sections for ST optical-fiber feedthroughs.

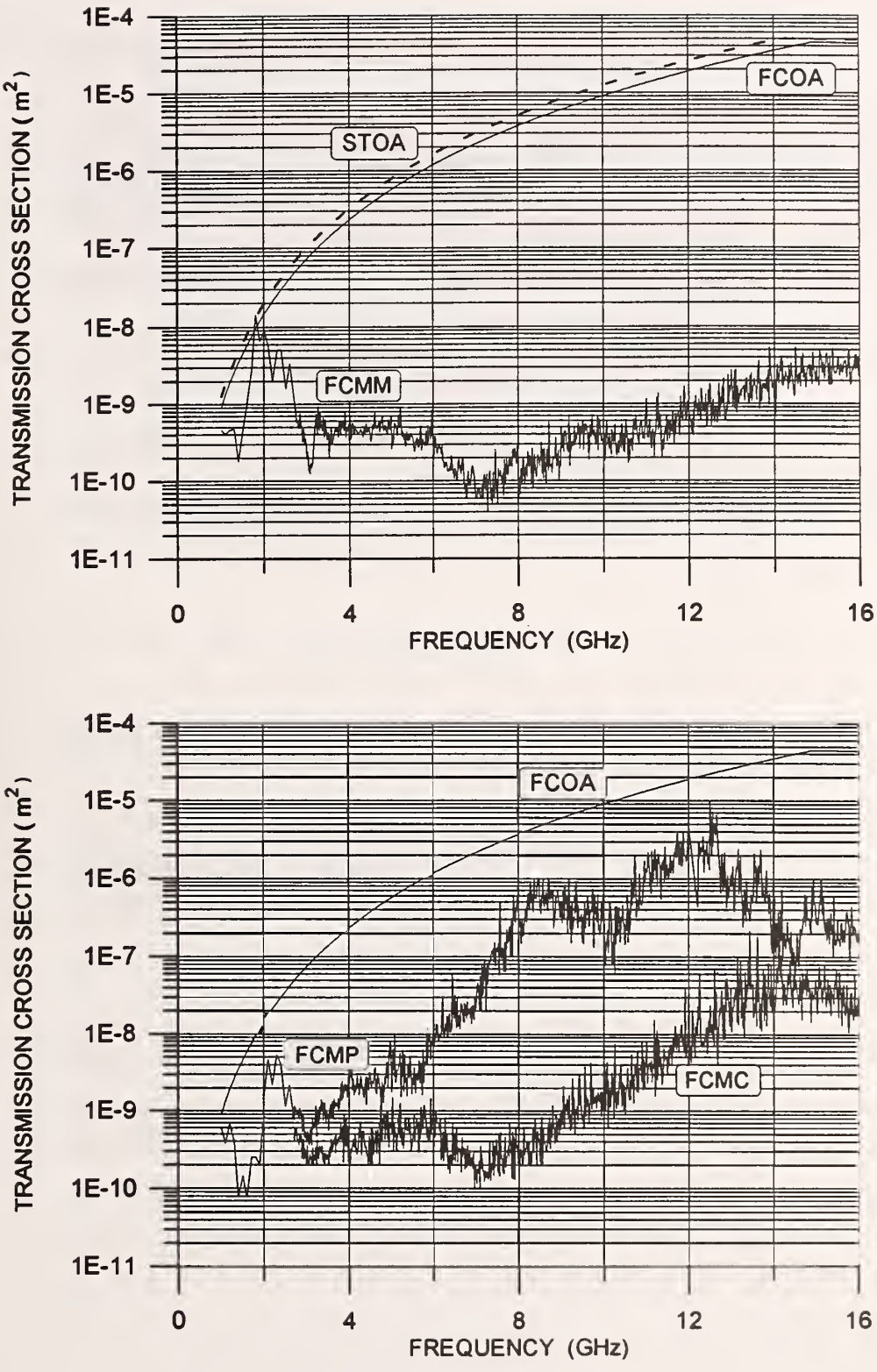

Figure 8. Transmission cross sections for FC/PC optical-fiber feedthroughs.

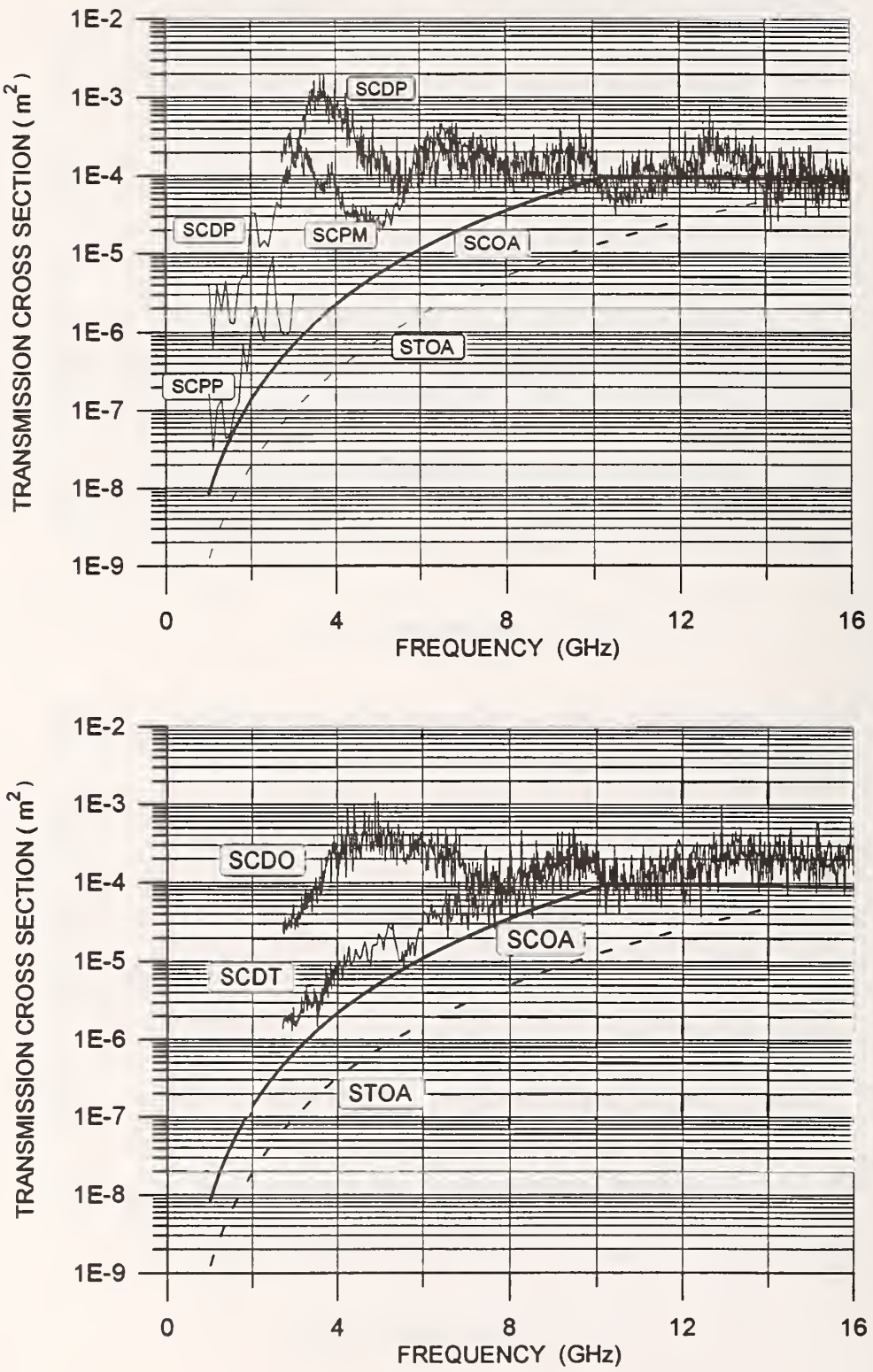

Figure 9. Transmission cross sections for SC optical-fiber feedthroughs.

5. UNCERTAINTY ANALYSIS

A proper uncertainty analysis is derived from eq (10), from which the transmission cross section is obtained. Standard techniques for the propagation of uncertainties [7] are used to obtain the combined standard uncertainty for the transmission cross sections. Differentiating eq (10) by parts, summing the squares of the terms, and dividing by eq (10), we obtain

$$\frac{u_c^2(\langle\sigma_T\rangle_{FT})}{\langle\sigma_T\rangle_{FT}^2} = \frac{u^2(\langle\sigma_T\rangle_{OA})}{\langle\sigma_T\rangle_{OA}^2} + \frac{u^2((S_I/S_C)_{OA})}{[(S_I/S_C)_{OA} - 1]^2} + \frac{u^2((S_I/S_C)_{FT})}{[(S_I/S_C)_{FT} - 1]^2} + \frac{[(S_I/S_C)_{OA} - (S_I/S_C)_{FT}]^2 u^2(F)}{[(S_I/S_C)_{OA} - 1]^2[(S_I/S_C)_{FT} - 1]^2 F^2} \quad (13)$$

for the fractional, mean square uncertainty in the measurand. We have used eq (11) to separate systematic errors due to the calibration constant F from the statistical fluctuations inherent in the data from the mode-stirred chamber. We have also concluded that the various component uncertainties are independent and uncorrelated. We discuss the various uncertainties below and provide details of the analysis along with the required partial derivatives of eq (10) and their spectral dependencies in Appendix B. Table 6 itemizes the various contributions to the combined fractional uncertainty and identifies whether they are derived from a statistical evaluation (Type A) or by some other method (Type B).

5.1 Uncertainty in the Reference Transmission Cross Section

Uncertainties in the cross section $\langle\sigma_T\rangle_{OA}$ for the open aperture which we use as a reference arise from the inadequacies in the electrically large and electrically small approximations. Previous studies [2] have shown these approximations to give good agreement with data for circular apertures at the high and low frequency ends of the spectrum. In the transition region for $ka = 1$ to $ka = 10$, minor resonance effects appear to be present. They are consistent with effects that have been evaluated theoretically for normal incidence by Levine and Schwinger [4]. Accurate data for all angles of incidence is not available in the literature. Figure B-1 shows the values and uncertainties that we used for the transmission cross section as a function of ka.

Table 5. Fractional component uncertainties for the transmission cross sections.

Source	Spectral dependence	Type	Maximum uncertainty rectangular distribution, dB		Standard uncertainty, dB
Reference cross section	Yes	B	1.5	$1 < ka < 4$	0.9
			0.8	otherwise	0.5
Signal ratio for reference aperture	calculated using covariance matrix				0.3
Fitting parameter A	Yes	A			3
Fitting parameter B	Yes	A			0.2
Fitting parameter C	Yes	A			0.6
Signal ratio for feedthrough	Yes	A			2
Calibration factor, F					0.3
Spectrum analyzer	No	B	0.5		0.3
Antenna transfer function	Yes	B	0.05		0.03
Cable loss *	Yes	B	0.1		0.05

* This does not include the uncertainty due to the faulty connector which we have added into the uncertainty in the signal ratios for the feedthroughs.

In the case of the rectangular apertures for the SC connectors, our experimental data for the simplex or single-fiber aperture was fit well by using a circular aperture of equivalent area. Numerical analysis of rectangular apertures [8] indicates that for $ka << 1$ the transmission cross section for the duplex connector would increase by about 1 dB over that of an equivalent circular aperture. Our data for the duplex connector were taken closer to $ka = 1$ and show considerably larger transmission cross sections, presumably due to resonance. As discussed above, we used the aperture for the single SC feedthrough also as the reference for all SC-duplex measurements. We think that the increase in the uncertainty for the transmission cross section measured for the SC-duplex feedthrough due to this choice is considerably less than 1 dB and is not significant compared to the uncertainties in the values for the reference aperture itself or to the statistical errors associated with $(S_I / S_C)_{FT}$.

5.2 Uncertainties in the Ratios for S_I / S_C

We use the analytical curve fitted to the $(S_I/S_C)_{OA}$ data for the computation of the transmission cross sections. The uncertainty in the curve is derived from a standard regression analysis for the correction term Q_4. The mean square uncertainty associated with $(S_I / S_C)_{OA}$ was calculated using the covariance matrix provided by the regression analysis and is plotted for the ST connector data in figure B-2. The residuals between the experimental data sets and the analytically fit curves show a small somewhat periodic dependence that appears to be correlated and reproduced in three of the four data sets. We can find no explanation for the observed dependence in the physics of the measurement technique and conclude the effect is characteristic of the instrumentation. Since a more sophisticated fitting routine would reduce the ripple and, therefore, the uncertainties in the analytic curves, the errors that we associate with $(S_I / S_C)_{OA}$ are conservative. Since they are also small compared to the total uncertainty for the transmission cross sections, there is no compelling reason to pursue a more sophisticated fit.

The probable errors in the $(S_I / S_C)_{FT}$ ratios for the connector feedthroughs are determined from the statistics of the spectral plots for the open apertures. The observed noise fluctuations are uniform across frequency and *SE*. We use the root-mean-square of the

residuals between the analytical curves fit to the open apertures and the actual data for the open aperture as the base uncertainty in these ratios. This is a conservative approach since it includes regions where the data for the open aperture are not centered about the fitted curve and thus would give a larger than appropriate mean-square result. In addition to the random noise attributed to the modal variations in reverberation chambers, the spectral plots we obtained show occasional jumps in the raw data at points where the frequency bands were changed. The jumps were more noticeable at the higher frequencies and on a few occasions amounted to about 6 dB. During the calibration of the signal cables at the end of the experiment, we discovered one cable had a loose connector. The observed jumps are consistent with changes in the reflection coefficient at the connector, which could occure if it was bumped and which become more prominent with increasing frequency. In the case of the measurements for the small open apertures, most of this discrepancy can be removed by adjusting the data to conform in shape to the theoretical model. Although spectral features in the data for the bulkhead feedthroughs made this more difficult, the corrections for most of jumps were still obvious. After correcting for these obvious jumps, we estimate that the uncertainty in $(S_I / S_C)^2_{FT}$ is a factor of 2 larger than the mean square of the residuals for the curve fit to the open apertures.

5.3 Uncertainties in the Calibration Factors

The uncertainties in the individual calibration factors are determined by manufacturers' specifications and NIST calibration data. They are identified along with the method used to estimate their numerical values in table 5. We calibrated the spectrum analyzers frequently using known input signals and obtain the calibration uncertainties given in table 5. These are about 1 dB below the manufacturer's specifications. The antennas are a closely matched pair, so $F_{1AF} / F_{2AF} \approx 1$, and systematic errors in their calibrated response should cancel. However, we used values provided by the manufacturer and considered each antenna separately to obtain a very conservative estimate for the uncertainty associated with the antenna factors.

The calibration of the coaxial cables on a network analyzer provides an uncertainty of about 0.5 dB. The error due to the faulty connector is not uniformly present in all the data and is

not considered to be a systematic error. Instead, we have included this effect in the uncertainty budget for $(S_I / S_C)_{FT}$ as reported above. The spectral dependence of the uncertainty associated with the calibration factor is shown in figure B-4. The contribution to the total error from systematic errors in the calibration factors is seen to be small. This is reasonable. Since almost all values of (S_I / S_C) are greater than 100, any systematic errors in these ratios nearly cancel from the numerator and denominator in eq (10).

5.4 Combined Standard Uncertainty

The component uncertainties are added according to eq (13) to obtain the combined standard mean-square fractional uncertainty for the transmission cross sections. We show the results for the fractional uncertainties for the ST connectors in figure B-5. The primary contribution to the uncertainty is from the large uncertainty associated with $(S_I / S_C)_{FT}$. The other significant contribution to the combined uncertainty is that associated with the theoretical values used for the transmission cross section of a small circular aperture. Since the major contributions to the combined uncertainty do not show strong spectral dependences, the final combined standard uncertainty shown in figure B-5 shows little spectral dependence. Although the resulting uncertainty is relatively large compared to those found in some measurement technologies, an uncertainty of ±3 dB is typical and acceptable in reverberation cell measurements. These results for the ST connectors are typical of all the data sets, and we assign a combined standard uncertainty of ±3 dB to all of the transmission cross sections reported.

6. CONCLUSIONS

The measured shielding effectiveness and transmission cross sections for the various connector styles and combinations show a wide range of values. We were able to achieve about 90 dB of shielding for the enclosure when a blank reference plate was used. The signal strengths for the bulkhead feedthroughs are sufficiently above the limits of the measurement

system to clearly show the relative performance of the various connector styles. Although the uncertainty in the measurements is in the range of ±3 dB, the differences between the various adapter barrel systems ranged from 10 to 30 dB. The results also clearly show the superiority of the FC metal/metal adapter for maintaining the integrity of a shielded enclosure.

We have successfully measured the ability of several optical-fiber bulkhead feedthrough systems in maintaining the shielding effectiveness of electronic enclosures. The results indicate that only the metal/metal systems are effective in maintaining the integrity of the enclosure. Several of the connector styles degraded the shielding even beyond that of the open aperture needed for their installation. This can be readily explained for the STMP system where a metal connector was used in conjunction with a dielectric adapter barrel. In this case the metal connector pair formed a dipole in the center of the aperture and efficiently coupled electromagnetic radiation into the enclosure. This also is the case for the SCPM measurement because of the metal alignment sleeve in the adapter barrel. The dielectric feedthrough systems such as those designated by STPP, SCPP, and SCDT are not completely dielectric. They have small metal springs between the outer shell and the ferrule to maintain pressure on and hold the ferrule securely in place. These small springs, together with the dielectric materials, which can act as flux concentrators, can also increase the coupling of radiation into the enclosure. In the case of the SC simplex connector system, an adapter barrel with a ceramic alignment sleeve was used for the low frequency measurement (SCPP), but the adapter used for the high frequency measurement (SCPM) had a metal alignment sleeve. A substantial increase in transmission cross section is evident at 3 GHz where we changed the adapter barrel.

The bottom set of curves in figure A-3 includes the measured SE for the open rectangular aperture required for the SC-duplex style connectors with (SCDT) and without (SCDO) a 1 mm wide piece of conducting tape across the center of the long dimension. The conducting strip considerably increases the shielding effectiveness at low frequencies, $ka < 1$, until it is just about one half of that for a single SC feedthrough. For applications that require SC-duplex connectors, we recommend that a feedthrough which accommodates a conducting strip be used. One way to accomplish this would be to use two separate single adapter barrels mounted with dimensions to match the duplex connectors.

We have obtained transmission cross sections for the tested systems. Together with other parameters of a specific enclosure, these transmission cross sections may be used to estimate the enclosure's shielding effectiveness. However, for small enclosures the geometry of the enclosure itself and its orientation with respect to ambient electromagnetic environment will also play an important a role in total leakage into the enclosure.

We have developed basic measurement techniques that can be used to test connector shielding effectiveness. The basic techniques can be applied to other types of devices and could be adapted to testing of active components such as connector mounted laser diodes and photodiodes.

There are areas in which measurement techniques could be improved to reduce the uncertainties reported here. Clearly, the faulty electrical connector was a problem that is easily corrected. Theoretical calculations and numerical analysis for the coupling of isotropic radiation, characteristic of that in the reverberation cell, through a small circular aperture would reduce the uncertainties in the reference cross sections. Finally, improved data-gathering techniques in which both signal processing channels could be synchronized to the tracking generator would reduce both the noise fluctuations and the data acquisition time.

7. ACKNOWLEDGEMENTS

The authors acknowledge J. Ladbury and D. Camell for considerable help in setting up the experimental equipment and data acquisition system. We also want to thank D. Hill for the helpful discussions throughout the project. KDM especially thanks D. Vecchia for valuable help in statistical and uncertainty analysis. We thank D. Kuchta and J. Crow of IBM for their suggestion to place a narrow strip of conducting tape across the aperture for the duplex SC adapter barrel in order to increase the shielding. Finally, we acknowledge the NIST Advanced Program Technology Office for financial support during part of the project.

8. REFERENCES

[1] Daher, J. Georgia Tech. Research Inst. Presentation at "Progress in Electromagnetic Research Symposium," U.S. Air Force Rome Laboratory. Contract F30602-89-C-0165, JPL; July 1993.

[2] Hill, D.A.; Ma, M.T.; Ondrejka, A.R.; Riddle, B.J; Crawford, M.L.; Johnk, R.T. Aperture Excitation of Electrically Large, Lossy Cavities. IEEE Trans. Electromagn. Compat., 36; 169-177; 1994.

[3] Meixner, J.; Andrejewski, W. Strenge theorie der beugung ebener elektromagnetischer wellen an der vollkommen leitenden kreisscheibe und an der kreisformigen offnung im vollkemmen leitenden eben schirm. Annalen der Physik. 7: 157-168; 1950.

[4] Levine, H.; Schwinger, J. On the theory of electromagnetic wave diffraction by an aperture in an infinite plane conducting screen. Comm. Pure Appl. Math. 3: 355-391; 1950.

[5] Crawford, M.L.; and Koepke, G.H. Design, evaluation, and use of a reverberation chamber for performing electromagnetic susceptibility/vulnerability measurements. Nat. Bur. Stand. (U.S.), Tech. Note 1092; 1986.

[6] Marquardt, D.W. An algorithm for least squares estimation of nonlinear parameters. J. Soc. Industrial Appl. Math. 2: 431-441; 1963.

[7] Taylor, B.N.; Kuyatt, C.E. Guidelines for Evaluating and Expressing the Uncertainty of NIST Measurement Results. Natl. Inst. Stand. Technol. Tech. Note 1297; 1994.

[8] de Meulenaere, F.; Van Bladel, J. Polarizability of Some Small Apertures. IEEE Trans. Antennas Propagat. AP-25: 198-205; 1977.

APPENDIX A. SHIELDING EFFECTIVENESS FOR OPTICAL-FIBER FEEDTHROUGHS

Figures A-1 through A-3 which compose this appendix, contain the shielding effectiveness curves for all the optical-fiber feedthroughs that were studied. They also contain the curves for the reference open apertures and their best fits derived from a standard regression analysis. The curve fit to the 9.5 mm open aperture is carried throughout the data set for comparison.

The shielding effectiveness values reported here are for our nested cell. The same values would not be obtained in a different experimental arrangement. They are used here for purpose comparison and to calculate the transmission cross sections.

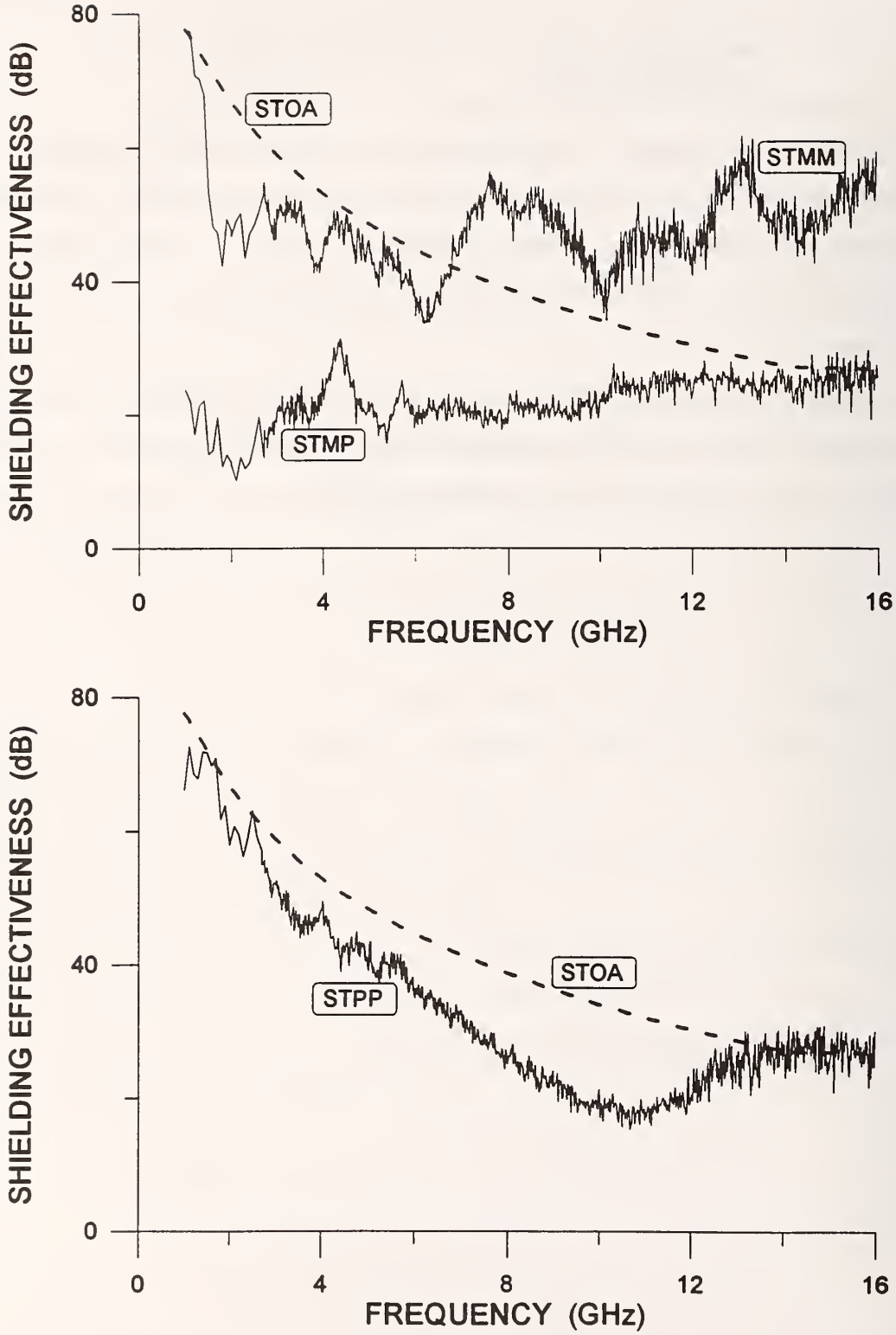

Figure A-1. Shielding effectiveness measured for ST optical-fiber feedthroughs.

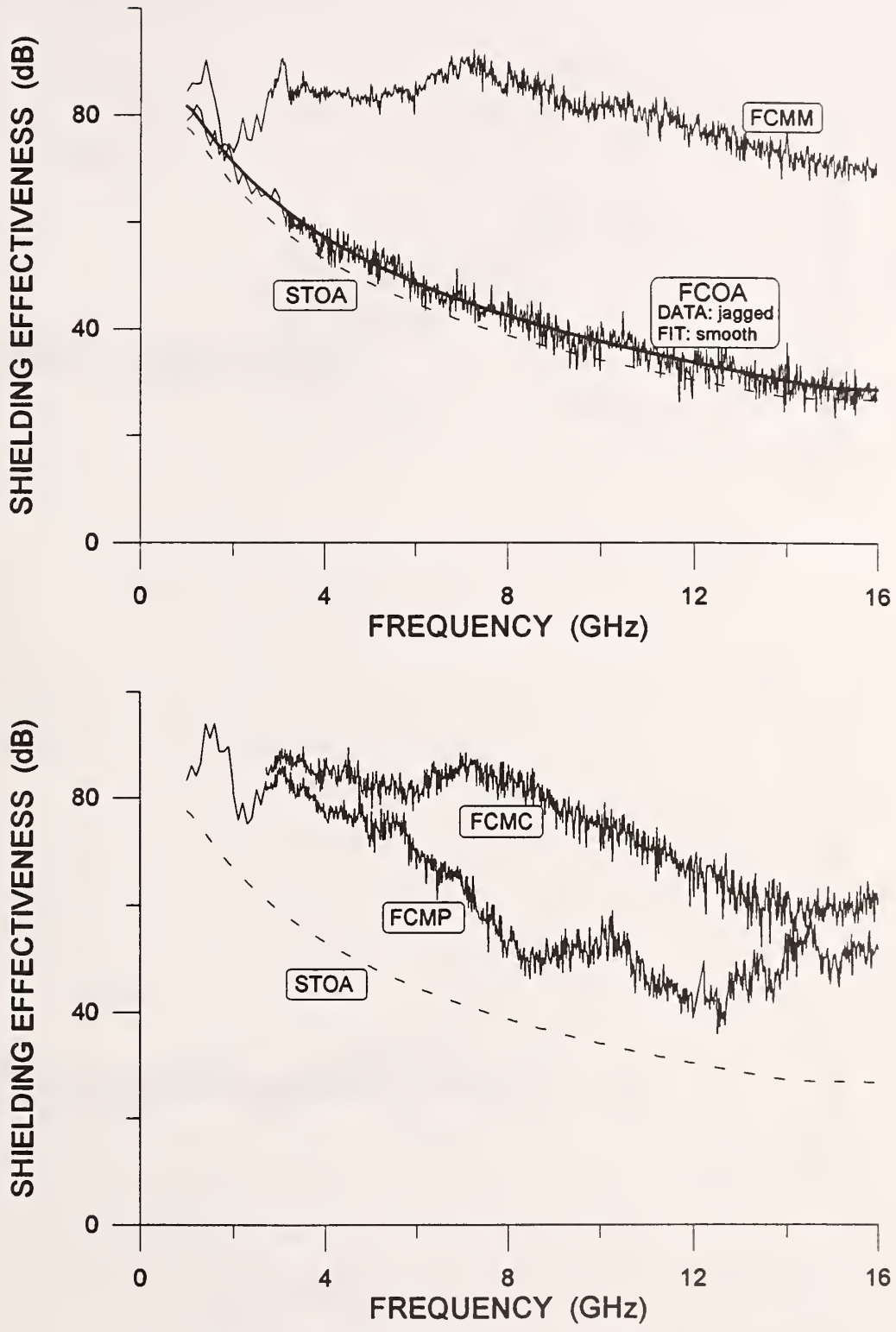

Figure A-2. Shielding effectiveness measured for FC/PC optical-fiber feedthroughs.

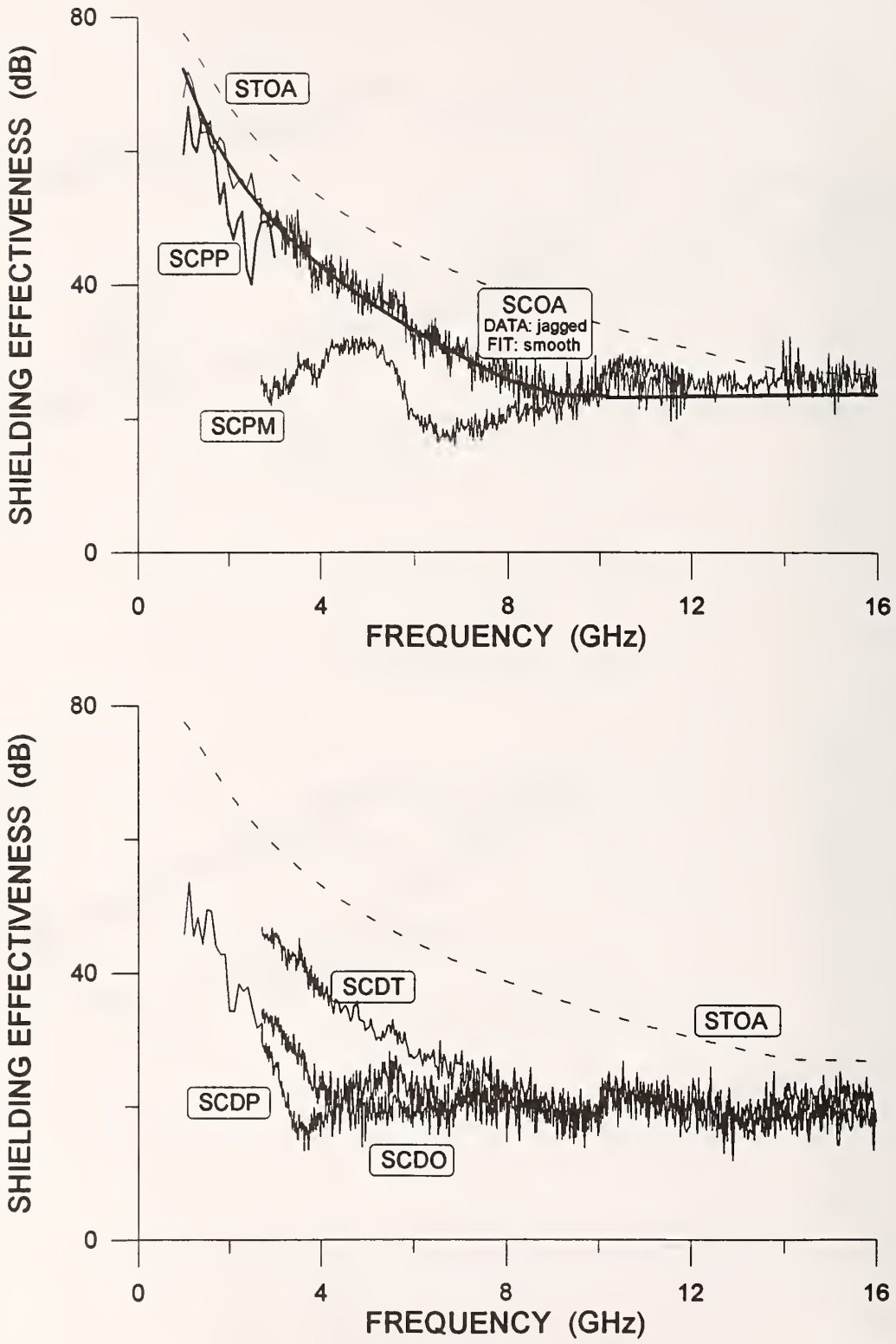

Figure A-3. Shielding effectiveness measured for SC optical-fiber feedthroughs.

APPENDIX B. SPECTRAL DEPENDENCE OF COMPONENT UNCERTAINTIES

In general, an estimate y of a measurand is determined from N other quantities through a functional relationship

$$y = f(x_1, x_2, x_3, \ldots x_N) , \tag{B-1}$$

where the x_i are the estimates for the N quantities. The uncertainties associated with the input estimates x_i are $u(x_i)$. When they are uncorrelated, the general rule for the propagation of uncertainties [8] can be written as

$$u_c^2(y) = \sum [c_i u(x_i)]^2 = \sum u_i^2(y) , \tag{B-2}$$

where $c_i = \partial f / \partial x_i$ is a sensitivity factor and $u_i(y) = |c_i| u(x_i)$. The $u_i(y)$ can be considered components of uncertainty of the measurement result y.

Using eq (10) and eq (11), we can rewrite the relationship between the unknown transmission cross section, the theoretical value for the transmission cross section of the open aperture, the measured signal ratios, and the calibration factor as

$$\langle \sigma_1 \rangle_{FT} = \langle \sigma_T \rangle_{OA} \frac{R_{OA} - F}{R_{FT} - F} . \tag{B-3}$$

This separates the systematic errors due to calibration factors into the one term F and the statistical fluctuations inherent in the experimental data of the mode-stirred chamber into the analyzer ratio term R. In the following figures, we give the analytical expressions, appropriate derivatives, and spectral plots for the components of standard fractional uncertainties.

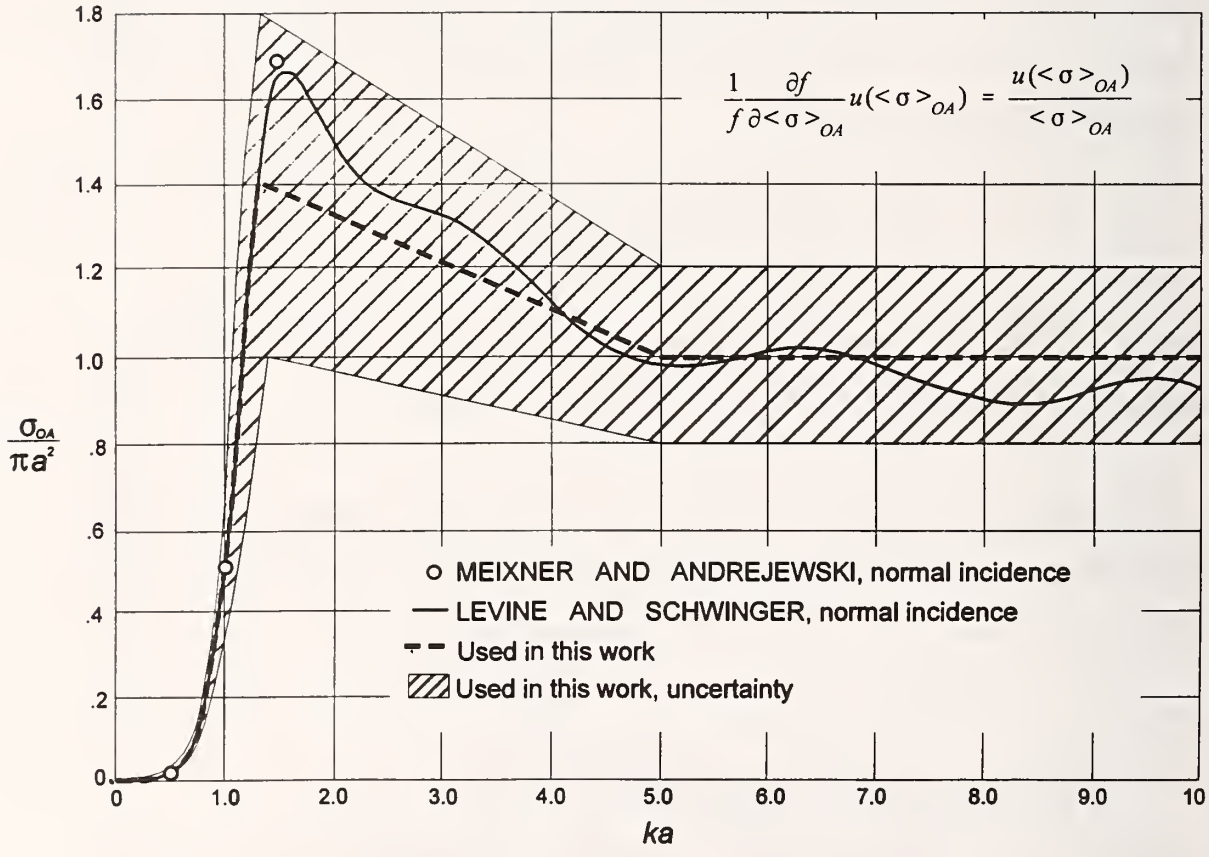

Figure B-1. Transmission cross section and fractional uncertainty for a circular aperture. The values are normalized to the electrically large limit given by eq (7).

$$\frac{1}{f}\frac{\partial f}{\partial R_{OA}}u(R_{OA}) = \frac{u(R_{OA})}{R_{OA}-F} = \frac{u((S_I/S_C)_{OA})}{(S_I/S_C)_{OA}-1}$$

$$u^2((S_I/S_C)_{OA}) = \sum_{ij} CM_{ij}\,\frac{\partial CF(x)}{\partial x_i}\,\frac{\partial CF(x)}{\partial x_j}$$

where CM = Covariance Matrix
$CF(x)$ = Analytical function for curve fit
x = Vector of fitting parameters (A, B, C)

$$\frac{\partial CF}{\partial A} = \frac{1}{k}\;;\quad \frac{\partial CF}{\partial B} = \frac{1}{k^2}\;;\quad \frac{\partial CF}{\partial C} = \frac{1}{k^3}$$

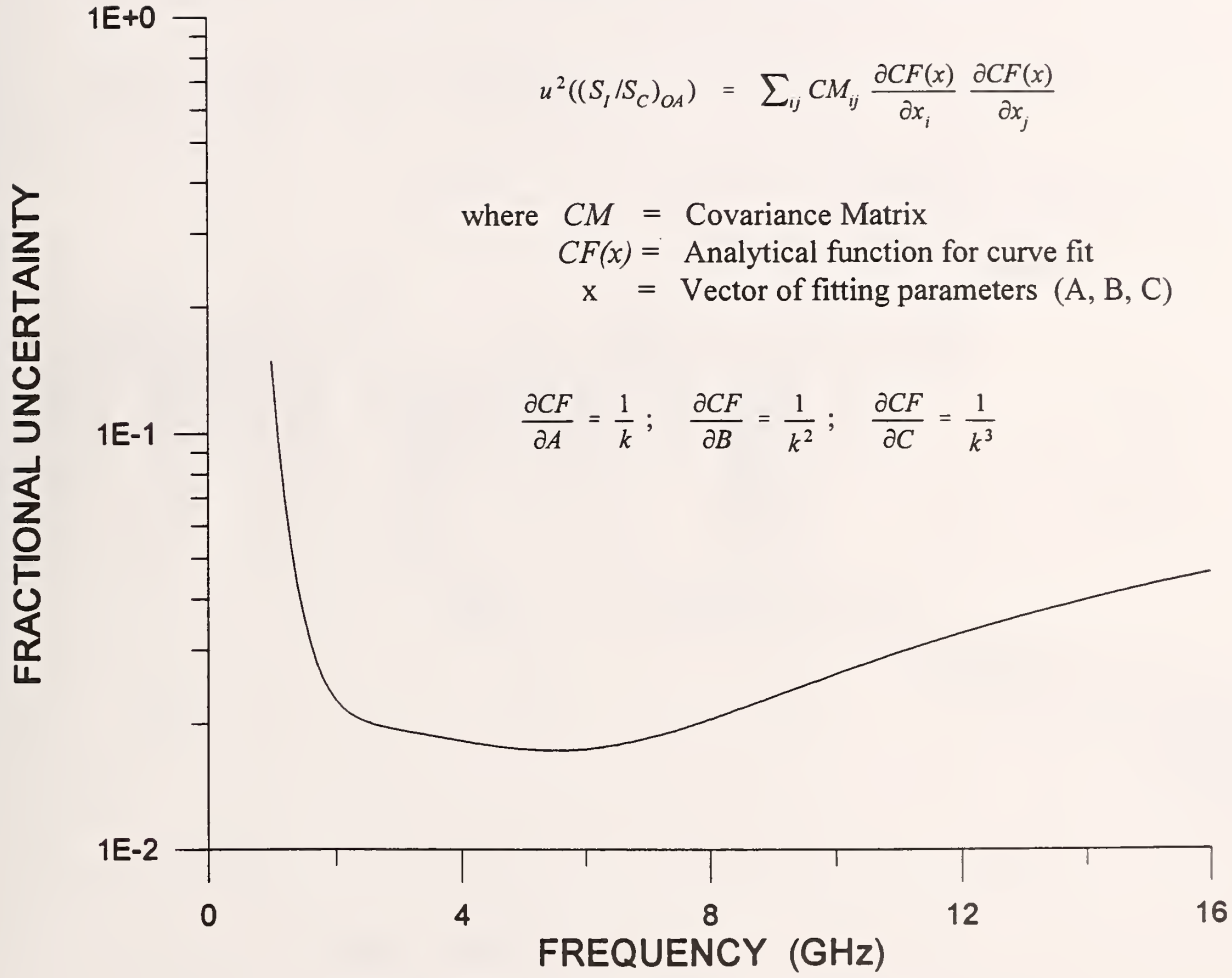

Figure B-2. Fractional uncertainty associated with the curve fit for $(S_I / S_C)_{OA}$.

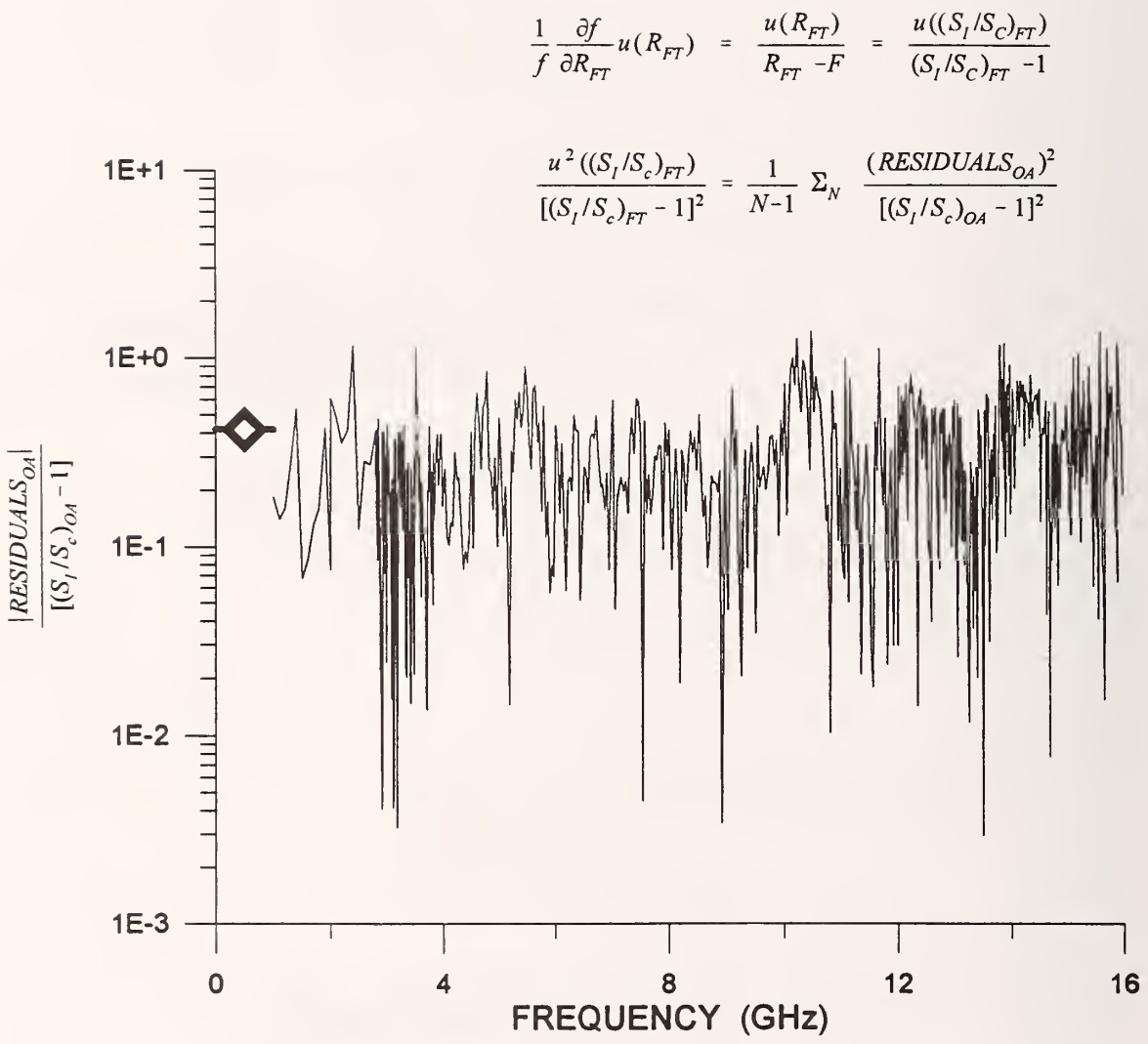

Figure B-3. Fractional uncertainty associated with $(S_I/S_C)_{FT}$. The residuals are the magnitude of the difference between the experimental data for the shielding effectiveness for the open aperture and the smooth analytic curve fit to the data. The diamond is the root-mean-square value and is equal to 0.418. We use this value times the square root of 2 for the fractional uncertainty associated with $(S_I/S_C)_{FT}$.

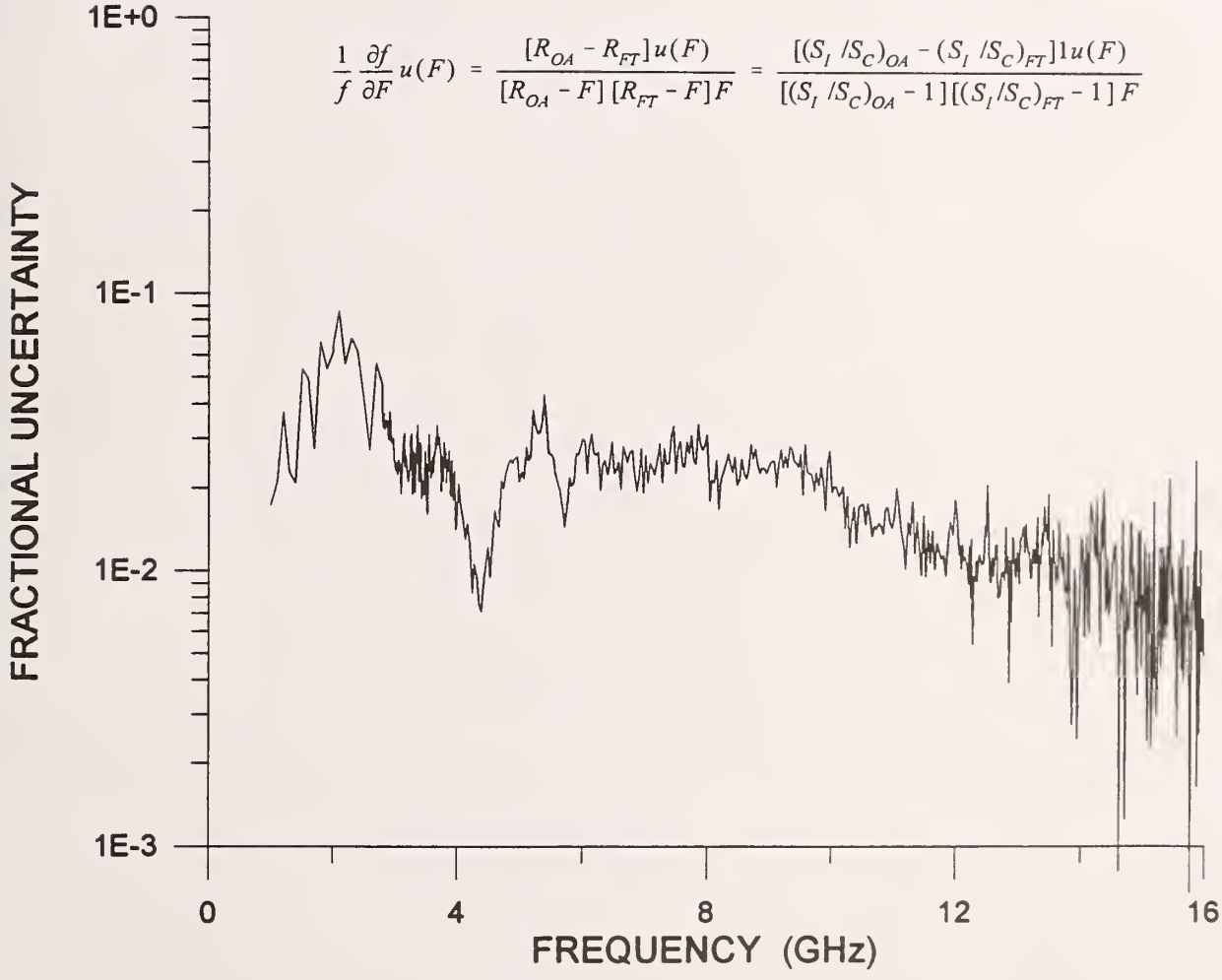

Figure B-4. Fractional uncertainty associated with the calibration factor.

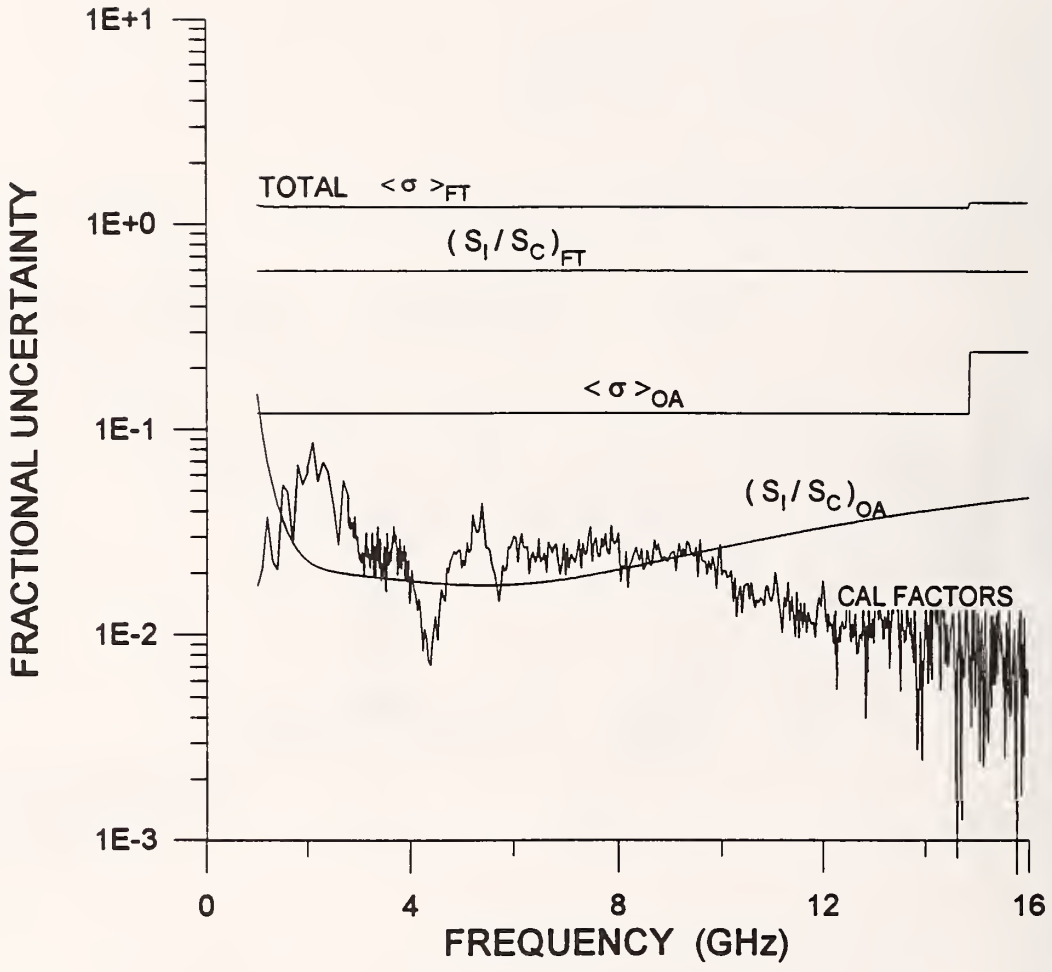

Figure B-5. Combined fractional uncertainty for the measured transmission cross sections. The result for $<\sigma_T>_{FT}$ is for a coverage factor of 2 corresponding to a 95% confidence interval.

• U.S. GOVERNMENT PRINTING OFFICE 1997-0-583-018/40049

NIST Technical Publications

Periodical

Journal of Research of the National Institute of Standards and Technology—Reports NIST research and development in those disciplines of the physical and engineering sciences in which the Institute is active. These include physics, chemistry, engineering, mathematics, and computer sciences. Papers cover a broad range of subjects, with major emphasis on measurement methodology and the basic technology underlying standardization. Also included from time to time are survey articles on topics closely related to the Institute's technical and scientific programs. Issued six times a year.

Nonperiodicals

Monographs—Major contributions to the technical literature on various subjects related to the Institute's scientific and technical activities.

Handbooks—Recommended codes of engineering and industrial practice (including safety codes) developed in cooperation with interested industries, professional organizations, and regulatory bodies.

Special Publications—Include proceedings of conferences sponsored by NIST, NIST annual reports, and other special publications appropriate to this grouping such as wall charts, pocket cards, and bibliographies.

Applied Mathematics Series—Mathematical tables, manuals, and studies of special interest to physicists, engineers, chemists, biologists, mathematicians, computer programmers, and others engaged in scientific and technical work.

National Standard Reference Data Series—Provides quantitative data on the physical and chemical properties of materials, compiled from the world's literature and critically evaluated. Developed under a worldwide program coordinated by NIST under the authority of the National Standard Data Act (Public Law 90-396). NOTE: The Journal of Physical and Chemical Reference Data (JPCRD) is published bimonthly for NIST by the American Chemical Society (ACS) and the American Institute of Physics (AIP). Subscriptions, reprints, and supplements are available from ACS, 1155 Sixteenth St., NW, Washington, DC 20056.

Building Science Series—Disseminates technical information developed at the Institute on building materials, components, systems, and whole structures. The series presents research results, test methods, and performance criteria related to the structural and environmental functions and the durability and safety characteristics of building elements and systems.

Technical Notes—Studies or reports which are complete in themselves but restrictive in their treatment of a subject. Analogous to monographs but not so comprehensive in scope or definitive in treatment of the subject area. Often serve as a vehicle for final reports of work performed at NIST under the sponsorship of other government agencies.

Voluntary Product Standards—Developed under procedures published by the Department of Commerce in Part 10, Title 15, of the Code of Federal Regulations. The standards establish nationally recognized requirements for products, and provide all concerned interests with a basis for common understanding of the characteristics of the products. NIST administers this program in support of the efforts of private-sector standardizing organizations.

Consumer Information Series—Practical information, based on NIST research and experience, covering areas of interest to the consumer. Easily understandable language and illustrations provide useful background knowledge for shopping in today's technological marketplace.

Order the **above** *NIST publications from: Superintendent of Documents, Government Printing Office, Washington, DC 20402.*

Order the **following** *NIST publications—FIPS and NISTIRs—from the National Technical Information Service, Springfield, VA 22161.*

Federal Information Processing Standards Publications (FIPS PUB)—Publications in this series collectively constitute the Federal Information Processing Standards Register. The Register serves as the official source of information in the Federal Government regarding standards issued by NIST pursuant to the Federal Property and Administrative Services Act of 1949 as amended, Public Law 89-306 (79 Stat. 1127), and as implemented by Executive Order 11717 (38 FR 12315, dated May 11, 1973) and Part 6 of Title 15 CFR (Code of Federal Regulations).

NIST Interagency Reports (NISTIR)—A special series of interim or final reports on work performed by NIST for outside sponsors (both government and non-government). In general, initial distribution is handled by the sponsor; public distribution is by the National Technical Information Service, Springfield, VA 22161, in paper copy or microfiche form.

U.S. Department of Commerce
National Institute of Standards and Technology
325 Broadway
Boulder, Colorado 80303-3328

Official Business
Penalty for Private Use, $300